Three-body bound states and structure calculations of the He_2-Ne system using the slow variable discretization method

Muhammad Saleem Shahzad and Yong Li*
Department of Physics, Huazhong Normal University, Wuhan 430079, China
(Received 22 May 2014; published 22 September 2014)

The He_2-Ne system with the combination of the isotopes of helium (^{3}He and ^{4}He) is used in structure calculations. Three-body channel functions and adiabatic potential functions have been calculated using the B-spline method. We use these channel functions in the slow variable discretization method to calculate the three-body bound states of the He_2-Ne system. Using this method, two bound states for the $^4He_2$-^{20}Ne system and one bound state for each of the ^{4}He-^{3}He-^{20}Ne and $^3He_2$-^{20}Ne systems have been found. The geometry of the trimer is also analyzed using the probability densities and expectation values.

DOI: 10.1103/PhysRevA.90.032510 PACS number(s): 31.15.xj, 36.90.+f

I. INTRODUCTION

There are many research works related to the weakly bound states of few-body systems to study some unusual properties of the systems, e.g., Efimov states and Halo states [1–3]. The Efimov state is the case when the two-body systems support only one bound state with a zero ground-state energy, but the three-body system supports an infinite number of bound states [4,5]. The other case is the halo or Borromean state, when the two-body systems do not have any bound state but the three-body system can have bound states. Since these three-body bound states have a binding energy of the order of mK to K, the system with weak interatomic forces becomes very important and relevant in the experimental and theoretical study of ultracold atomic collisions and Bose-Einstein condensates in various aggregations.

The calculation of these weakly bound states has been problematic due to their anharmonic potential surface and large amplitude, implying floppy and delocalization motion of these systems. To overcome these problems, the adiabatic hyperspherical coordinate system is used, which simplifies the problem of calculating the three-body bound states [1,2]. This is simple in methodology but suffers from numerical instability when the system has a large number of the sharp avoided crossings in the adiabatic channel functions. Due to these instabilities it was not easy to analyze most of the practical systems and the study was limited to simple trimers such as He_3 and its hydrides [1,3,6,7]. These avoided-crossing numerical instabilities can be removed by changing the representation method of the Hamiltonian from adiabatic to diabatic and maintaining the smoothness in the adiabatic variable, which in our case is the hyperradius R. There is an approach called the diabatic by sector method, which was also applied to scattering problems [8,9]. There is a method proposed by Tolstikhin *et al.* called slow variable discretization (SVD) [10], which allows the separation of the adiabatic variables in the Hamiltonian and results in smoothness in the adiabatic variable R. Many authors used this approach successfully to analyze various triatomic systems [10–14]. We also use the SVD approach to study the He_2-Ne triatomic system.

In the present work the hyperspherical coordinate system is used, proposed by Macek [15] and later comprehensively reviewed by Lin [2], along with the SVD approach. We calculate the results for the above-mentioned trimers with the ^{3}He and ^{4}He isotopes. The empirical pair potentials for the He-He and He-Ne dimers are used to calculate the three-body potential surface [16,17]. First, the channel functions are calculated by selecting a suitable grid for convergent results at minimum possible grid points to optimize the calculation time and then, using these channels and potential functions, the three-body bound states are calculated. The various features of the channel functions and the average distances between the atoms of the trimers in different bound states are also discussed.

II. THEORETICAL METHOD

We treat the He_2-Ne molecule as a three-body system. Since the purpose of the present work is to see if there are bound states of the He-He-Ne triatomic system, we consider only the most favorable condition for the lowest states of the He-He-Ne molecules with the angular momentum $J = 0$. We solve the Schrödinger equations for these three-body systems using well-established hyperspherical coordinates in the adiabatic approximation. The channel functions and adiabatic three-body potential curves are obtained by this method. A detailed description of the calculation method is given in Ref. [18].

We use the Jacobi coordinate method in the center-of-mass frame to solve the Schrödinger equation and we choose two helium atoms as atoms 1 and 2 and neon as the third atom in our three-body system. In the center-of-mass frame, ρ_1 is used as the first Jacobi coordinate from atom 1 to atom 2 with the reduced mass μ_1 and ρ_2 as the second Jacobi coordinate from the center of mass of atoms 1 and 2 to the third atom with the reduced mass μ_2. Here θ is the angle between ρ_1 and ρ_2. The hyperradius R and hyperangle ϕ are defined as

$$\mu R^2 = \mu_1 \rho_1^2 + \mu_2 \rho_2^2, \tag{1}$$

$$\tan\phi = \sqrt{\frac{\mu_2}{\mu_1}}\frac{\rho_2}{\rho_1}, \tag{2}$$

$$\cos\theta = \frac{\vec{\rho}_1 \cdot \vec{\rho}_2}{\rho_1 \rho_2}, \tag{3}$$

*Corresponding author: yongli@phy.ccnu.edu.cn

TABLE I. Two-body bound-state energies (in K) of the ^{4}He-^{20}Ne and ^{3}He-^{20}Ne systems using the TT potential [17].

(v,J)	^{4}He-^{20}Ne E (K)	^{3}He-^{20}Ne E (K)
(0,0)	–3.43349	–2.34370
(0,1)	–2.44319	–1.22916
(0,2)	–0.58195	

where μ is an arbitrary scaling factor. In our calculation we select $\mu = \sqrt{\mu_1\mu_2}$. We use atomic units throughout our calculations unless stated otherwise. As we consider the states with $J = 0$ only, the Schrödinger equation involves only three internal coordinates R, ϕ, and θ. The Schrödinger equation written in terms of the rescaled wave function $\psi(R,\phi,\theta) = \Psi(R,\phi,\theta)R^{3/2}\sin\phi\cos\phi$ is [2,10]

$$\left(-\frac{1}{2}\frac{\partial}{\partial R}R^2\frac{\partial}{\partial R} + H_{\rm ad}(R,\phi,\theta)\right)\psi(R,\phi,\theta) = R^2E\psi(R,\phi,\theta), \tag{4}$$

with

$$H_{\rm ad}(R,\phi,\theta) = \frac{\Lambda^2 - \frac{1}{4}}{2} + R^2V(R,\phi,\theta) \tag{5}$$

and

$$\Lambda = -\frac{\partial^2}{\partial\phi^2} - \frac{1}{\sin^2\phi\cos^2\phi\sin\theta}\frac{\partial}{\partial\phi}\left(\sin\theta\frac{\partial}{\partial\theta}\right). \tag{6}$$

Then the adiabatic potentials $U_v(R)$ and channel functions $\Phi_v(R,\phi,\theta)$ at a fixed R are obtained by solving

$$H_{\rm ad}\Phi_v(R,\phi,\theta) = U_v(R)\Phi_v(R,\phi,\theta). \tag{7}$$

To solve Eq. (7) we use the B-spline basis functions [19]. Using the B-spline basis functions, the channel functions can

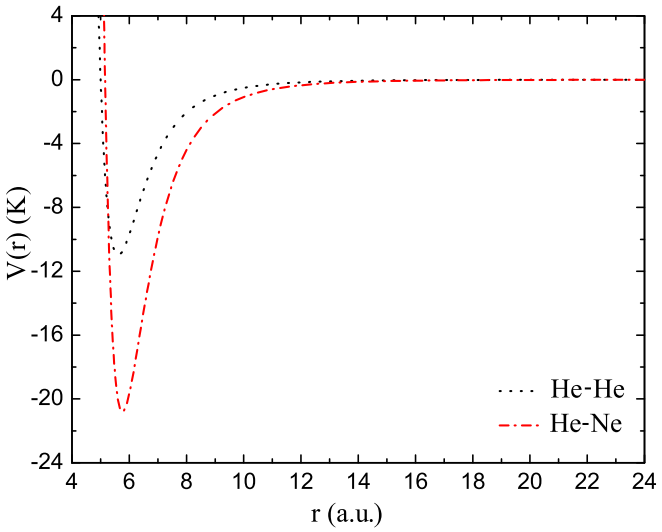

FIG. 1. (Color online) Potential energy curves for the He-He (dotted line) and He-Ne (dash-dotted line) pairs. The pair potential for He-He is taken from Ref. [16] and He-Ne is the revised TT potential from Ref. [17].

TABLE II. Test of the convergence for some of the lowest hyperspherical potentials (in K) at the hyperradius $R = 100$ with respect to the number of basis sets for ϕ and θ in the ^{4}He$_2$-^{20}Ne and ^{3}He$_2$-^{20}Ne system calculations.

	^{4}He$_2$-^{20}Ne			^{3}He$_2$-^{20}Ne	
(N_ϕ,N_θ)	$v=1$	$v=2$	$v=3$	$v=1$	$v=2$
(90,40)	–3.257	–2.010	–0.1738	–2.210	–0.943
(90,50)	–3.257	–2.010	–0.1739	–2.210	–0.943
(130,50)	–3.416	–2.362	–0.5044	–2.333	–1.188
(150,50)	–3.437	–2.413	–0.5440	–2.351	–1.215
(165,50)	–3.444	–2.437	–0.5621	–2.356	–1.228
(170,50)	–3.447	–2.442	–0.5696	–2.358	–1.229
(175,50)	–3.447	–2.444	–0.5695	–2.358	–1.231
(175,55)	–3.447	–2.444	–0.5696	–2.358	–1.231

be expressed in the form

$$\Phi_v(R,\varphi,\theta) = \sum_i^{N_\varphi}\sum_j^{N_\theta} c_{i,j}^v(R)B_i(\varphi)B_j(\theta) \tag{8}$$

and the boundary conditions are

$$\Phi_v(R,0,\theta) = \Phi_v\left(R,\frac{\pi}{2},\theta\right) = 0 \tag{9}$$

and

$$\left.\frac{\partial\Phi_v(R,\phi,\theta)}{\partial\theta}\right|_{\theta=0} = \left.\frac{\partial\Phi_v(R,\phi,\theta)}{\partial\theta}\right|_{\theta=\pi} = 0, \tag{10}$$

where N_ϕ and N_θ are the sizes of the basis set in ϕ and θ coordinates, respectively. The B-spline basis set is used because of its high localization property, flexibility, and high numerical stability. As a result, the Hamiltonian and overlap matrix both are banded and can be solved easily using the standard LAPACK routines for generalized eigenvalues problems.

Equation (4) is solved by using the SVD method proposed by Tolstikhin *et al.* [10]. Its solution $\psi(R,\phi,\theta)$ can be expanded as the pointwise discrete variable representation (DVR) basis functions $\pi_j(R)$,

$$\psi(R,\varphi,\theta) = \sum_{j=1}^{N_{\rm DVR}}\sum_{\mu=1}^{N_\mu} c_{j\mu}\pi_j(R)\Phi_\mu(R_j,\varphi,\theta), \tag{11}$$

where $N_{\rm DVR}$ and N_μ are the dimensions of the DVR basis functions $\pi_j(R)$ and the number of coupled channels, respectively. The DVR basis functions $\pi_j(R)$ are constructed from the Gauss-Laguerre polynomials $L_n^\alpha(R/\beta)$ with $\alpha = 3$ and the scaling factor $\beta = R_{\rm max}/R_N$. Now the hyperradial Schrödinger equation (4) can be written as

$$\sum_{j=1}^{N_{\rm DVR}}\sum_{\mu=1}^{N_\mu}(K_{ij} - E\rho_{ij})O_{iv,j\mu}c_{j\mu} + U_v(R_i)c_{iv} = 0, \tag{12}$$

where

$$K_{ij} = -\frac{1}{2\mu}\int_0^\infty \pi_i(R)\left(\frac{\partial}{\partial R}R^2\frac{\partial}{\partial R}\right)\pi_j(R)dR, \tag{13}$$

$$\rho_{ij} = \int_0^\infty \pi_i(R)R^2\pi_j(R)dR, \tag{14}$$

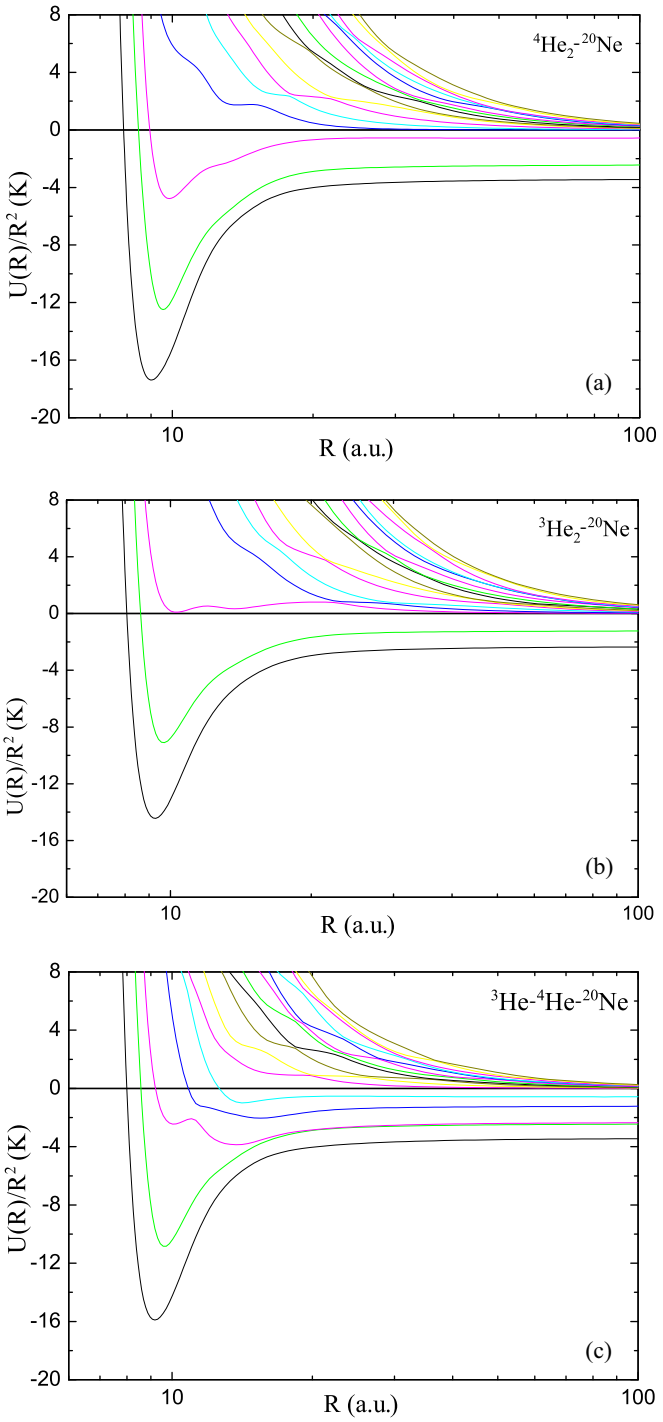

FIG. 2. (Color online) (a) Adiabatic hyperspherical potential curves of the $^4He_2$-^{20}Ne system including several channels. (b) Adiabatic hyperspherical potential curves of the $^3He_2$-^{20}Ne symmetric system including several channels. (c) Adiabatic hyperspherical potential curves of the ^3He-^4He-^{20}Ne system including several channels.

and

$$O_{iv,j\mu} = \langle \Phi_v(R_i,\phi,\theta)|\Phi_\mu(R_j,\phi,\theta)\rangle. \qquad (15)$$

TABLE III. Test of the convergence for the bound states (in K) of the $^4He_2$-^{20}Ne and $^3He_2$-^{20}Ne systems with respect to the number of DVR basis sets and the number of channels included in thecalculations.

(N_{DVR}, N_μ)	$^4He_2$-^{20}Ne		
$v=0$	$v=1$	$v=0$	$^3He_2$-^{20}Ne
(50,10)	–7.246	–4.407	–4.819
(60,10)	–7.245	–4.406	–4.818
(60,16)	–7.266	–4.431	–4.836
(60,20)	–7.271	–4.437	–4.840
(60,24)	–7.274	–4.439	–4.843
(70,24)	–7.274	–4.439	–4.842
(70,26)	–7.275	-4.440	–4.844

Here $O_{iv,j\mu}$ is the overlap matrix between two adiabatic channels defined at different Gauss-Laguerre quadrature points in R and integrated over ϕ and θ.

III. RESULTS AND DISCUSSION

A. Two-body potentials and bound states

In our calculation the three-body potential obtained by adding the two-body pair potentials is used as

$$V_{add} \cong [V_{He\text{-}He}(r_{12}) + V_{He\text{-}Ne}(r_{13}) + V_{He\text{-}Ne}(r_{23})]. \qquad (16)$$

The three-body interaction potential is not considered in the present calculations as it has been shown to have a less than 1% effect on the He_3 ground-state energy [20,21]. For the He-He pair we use the two-body potential suggested by Aziz and Slaman [16], which is well established and most commonly used by many researchers [22–26]. Using this potential we get the only one bound state for ^4He-^4He with an energy of -1.31 mK and no bound state for ^3He-^4He. For the He-Ne pair we select the interatomic van der Waals Tang-Toennies (TT) potential [17], which is currently the most recent and revised potential. This potential is based on the TT potential model and uses the combining rule derived in their earlier work. This potential is based on the updated input data and the difference from the empirical data is now less than 1% [27]. Using this potential for ^4He-^{20}Ne, we find the ground state ($v=0, j=0$) of -3.4335 K ($-2.3864\,cm^{-1}$), which is in good agreement with the reported bound state [12,25]. We find the three bound states for the ^4He-^{20}Ne dimer using this potential. Additional bound states with nonzero j are listed in Table I. Two-body potentials for the He-He and He-Ne dimers are shown in Fig. 1.

TABLE IV. Calculated three-body bound states (in K) of the He_2-Ne system with the different He isotopes.

v	$^4He_2$-^{20}Ne	$^3He_2$-^{20}Ne	^3He-^4He-^{20}Ne
0	–7.275	–4.844	–6.032
1	–4.440		

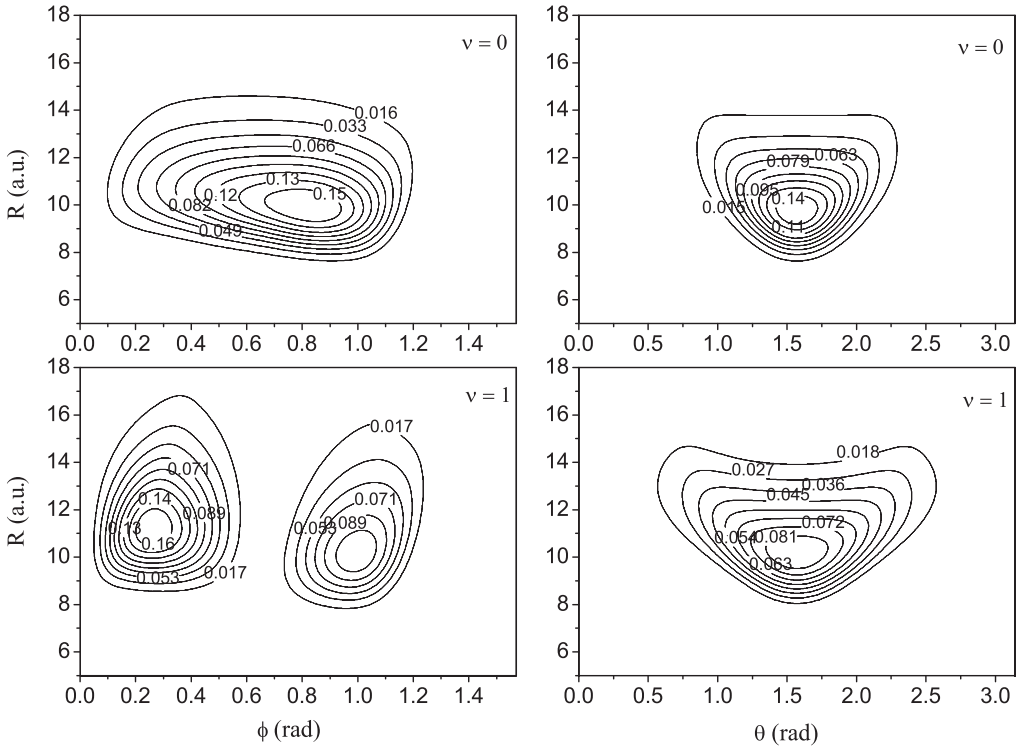

FIG. 3. Contour plots of the two-dimensional probability density functions for all the bound states of the $^4He_2$-^{20}Ne trimer integrated over θ (left) and over ϕ (right).

B. Hyperspherical potential curves and channel functions

Using the B-spline basis we solve Eq. (4) and calculate the channel function $\Phi(R,\phi,\theta)$ and the adiabatic potential functions U_v. We select N_ϕ and N_θ so that these potential curves converge to a reasonable accuracy and perform the convergence test for the hyperspherical channel for a different kind of grid and number of grid points, suggested in Ref. [28], along with a small modification according to our problem.

For the $^4He_2$-^{20}Ne and $^3He_2$-^{20}Ne symmetric systems, the exponential grid for the ϕ coordinate and the sinusoidal grid for the θ coordinate are used. For the ^{3}He-^{4}He- ^{20}Ne system, the symmetric exponential grid starts from the middle for the ϕ coordinate. We perform the convergence test at the different values of R. The convergence of the adiabatic channel potentials is very fast for small values of R and slower for higher values of R. We choose $R = 20$ and 100 a.u. for the convergence test. The convergence results at $R = 100$ a.u. are shown in Table II. The limiting value of R in the final calculation is 100 a.u. We select $N_\phi = 170$ and $N_\theta = 70$ for the symmetric systems (^{4}He-^{4}He-^{20}Ne and ^{3}He-^{3}He-^{20}Ne) and $N_\phi = 170$ and $N_\theta = 130$ for the asymmetric system (^{3}He-^{4}He- ^{20}Ne) for the final calculations. The three-body adiabatic hyperspherical potential curves are shown in Fig. 2, which includes the avoided crossings. We can see the convergence of the potential curves at the higher value of R to the dissociation energy of the trimers, which is the binding energy of the dimers. For the $^4He_2$-^{20}Ne system these are the lowest three channels and for the $^3He_2$-^{20}Ne

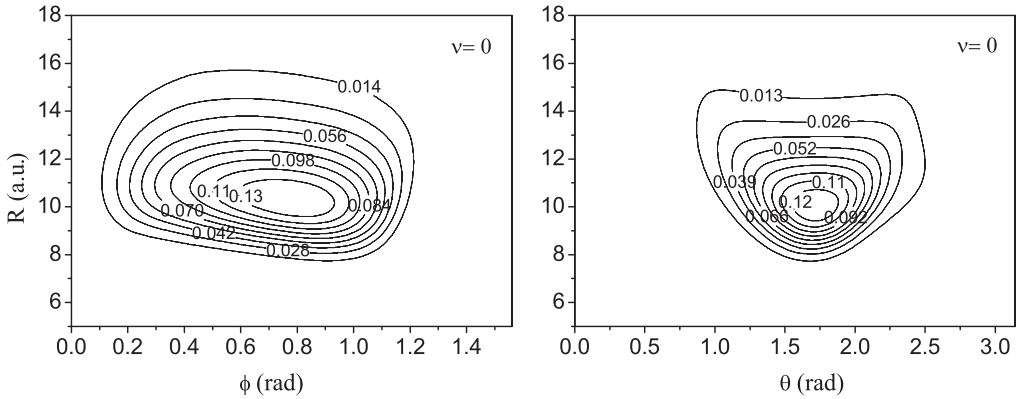

FIG. 4. Contour plots of the two-dimensional probability density function for the bound state of the ^{3}He-^{4}He-^{20}Ne trimer integrated over θ (left) and over ϕ (right).

system there are only two, depending on the number of bound states of the respective dimers. However, for the asymmetric ^{4}He-^{3}He-^{20}Ne system, it has five channels, which include the three bound states of the ^{4}He-^{20}Ne dimer and the two bound states of the ^{3}He-^{20}Ne dimer. Here the channel corresponding to the ^{4}He$_2$ dimer bound state is not visible in Fig. 2 as its binding energy is very small compared to other channels.

C. Three-body bound states

The three-body bound states are calculated from Eq. (12) using the Gauss-Laguerre DVR basis. The bound states converge with increasing number of DVR basis sets and the number of coupled channels included in the calculations. Table III shows the convergence of the test results of the bound states of the ^{4}He$_2$-^{20}Ne and ^{3}He$_2$-^{20}Ne systems. The convergence is fast with an increasing number of basis sets and coupled channels. We use $N_{\rm DVR} = 70$ and $N_\mu = 26$ in our final calculation to get at least four significant digit convergence.

For the ^{4}He$_2$-^{20}Ne system one ground state of -7.275 K and one excited state of -4.440 K are found. For the ^{3}He$_2$-^{20}Ne and ^{3}He-^{4}He-^{20}Ne systems, the three-body potential is shallower than that of the ^{4}He$_2$-^{20}Ne system because, due to the lower mass of the ^{3}He, there exist only ground bound states of -4.844 and -6.032 K for these two trimers respectively and no excited state. All the bound states are listed in Table IV.

D. Probability densities and structure of the three-body system

To illustrate the structure of the three-body system we calculate the total wave function for each bound state. In Fig. 3 the two-dimensional results are presented for the density function of the ^{4}He$_2$-^{20}Ne system in the first and second columns, integrated over θ and ϕ, respectively. The first row includes the probability densities for the ground state and the second row includes the probability densities of the excited state.

The maximum for the probability density is at $(R,\phi,\theta) =$ (9.8 a.u., 0.83 rad, 1.57 rad) for the ground state of the ^{4}He$_2$-^{20}Ne system, which is the isosceles triangle structure when translated to the interatomic distances and also an expected result due to the symmetric system. For the excited state there are two maxima for the probability density. The principle maximum is at $(R,\phi,\theta) =$ (11.1 a.u., 0.26 rad, 1.57 rad), which is almost a linear structure. The second maximum is at $(R,\phi,\theta) =$ (9.8 a.u., 0.99 rad, 1.57 rad), which is an equilateral triangle. We do not include the ^{3}He$_2$-^{20}Ne density plots in the paper as they are qualitatively similar to the ^{4}He$_2$-^{20}Ne system.

For the asymmetric system ^{3}He-^{4}He-^{20}Ne, there is just one bound state. Figure 4 shows the two-dimensional plots of the probability density for the ground state. The first column shows the probability density integrated over θ and in the second column it is integrated over ϕ. The maximum for the probability density is at $(R,\phi,\theta) =$ (10.28 a.u., 0.78 rad, 1.70 rad) for the ground state, which is a scalene triangle. The probability density plots also show the asymmetric behavior of the trimer.

TABLE V. Calculated average values of the different parameters for all the bound states of the ^{4}He$_2$-^{20}Ne, ^{3}He$_2$-^{20}Ne, and ^{3}He-^{4}He-^{20}Ne trimers.

	^{4}He$_2$-^{20}Ne		^{3}He$_2$-^{20}Ne	^{3}He-^{4}He-^{20}Ne
$(N_{\rm DVR}, N_\mu)$	$v=0$	$v=1$	$v=0$	$v=0$
$\langle r_{12}\rangle$	10.65	12.08	11.88	11.29
$\langle r_{12}^2\rangle^{1/2}$	11.06	12.76	12.39	11.75
$\langle r_{23}\rangle$	7.61	8.10	8.24	7.62
$\langle r_{23}^2\rangle^{1/2}$	7.74	8.28	8.43	7.81
$\langle r_{31}\rangle$				8.22
$\langle r_{31}^2\rangle^{1/2}$				8.50
$\beta_{\rm Ne}$	91.5°	102.9°	94.9°	93.5°
$\langle\cos\beta_{\rm Ne}\rangle$	–0.03	–0.22	–0.08	–0.06
$\langle R\rangle$	10.96	11.88	11.93	11.44
$\langle R^2\rangle^{1/2}$	11.10	12.08	12.15	11.62

Calculations are also preformed for the average magnitude of the distance between the atoms and the bond angle between them. For the nth bound state, the average distance r_{ij} between atoms i and j can be calculated as

$$\langle r_{ij}\rangle_n = \int dR \int d\Omega \psi_n^*(R,\Omega) r_{ij} \psi_n(R,\Omega), \qquad (17)$$

with $\Omega = (\phi,\theta)$.

The average value of the cosine of the bond angle of atom j using the cosine law is

$$\langle\cos\beta_j\rangle_n = \int dR \int d\Omega \psi_n^*(R,\Omega) \frac{r_{ij}^2 + r_{jk}^2 - r_{ki}^2}{2 r_{ij}^2 r_{jk}^2} \psi_n(R,\Omega). \qquad (18)$$

Here ijk are the cyclic permutations of (1,2,3). The calculated results for the interatomic distance and bound angle are presented in Table V. When atoms 1 and 2 are the same, the symmetry of the system leads r_{23} and r_{31} to be the same, so only one of them is calculated. The interatomic distance is dependent on the bond strength between the atoms. So the stronger the bond, the shorter the distance is between the atoms, which is evident from the results. The average distance between the He-Ne atoms is much shorter than that between the He-He atoms because of the stronger bonding between the He-Ne atoms.

IV. SUMMARY

In the present work we performed calculations for the three-body bound states of the He$_2$-Ne system using the slow variable discretization method. Along with the discrete variable representation, this method was selected to avoid the numerical difficulties arising from the use of the hyperspherical representations. This method is very effective for three-body bound-state calculations especially when the three-body channel functions have avoided crossings. In these calculations we found two bound states for the ^{4}He$_2$-^{20}Ne system and one bound state for each of the ^{3}He$_2$-^{20}Ne and ^{3}He-^{4}He-^{20}Ne

systems. Furthermore, to understand the geometry of the trimer, the wave functions along with probability densities were studied qualitatively and quantitatively. The average interatomic distances and bond angles were also reported. Since the He_2-Ne system has binding energies on the order of 1 K, these weakly bound molecules can exist only in a cold environment. Using laser cooling and other cooling methods for atoms and molecules, it may be possible to perform direct observations of these molecules. Our results can be used to provide some guidance for experimentalists in their search for such weakly bound molecules.

ACKNOWLEDGMENTS

We acknowledge the financial support provided by the China Scholarship Council. This work was supported by the National Natural Science Foundation of China under Grant No. 10974064.

[1] B. D. Esry, C. D. Lin, and C. H. Greene, Phys. Rev. A **54**, 394 (1996).
[2] C. D. Lin, Phys. Rep. **257**, 1 (1995).
[3] H. Suno and B. D. Esry, Phys. Rev. A **78**, 062701 (2008).
[4] V. Efimov, Phys. Lett. B **33**, 563 (1970).
[5] V. Efimov, Nucl. Phys. A **210**, 157 (1973).
[6] D. Blume, C. H. Greene, and B. D. Esry, J. Chem. Phys. **113**, 2145 (2000).
[7] H. Suno and B. D. Esry, Phys. Rev. A **82**, 062521 (2010).
[8] R. T. Pack and G. A. Parker, J. Chem. Phys. **87**, 3888 (1987).
[9] B. K. Kendrick, R. T. Pack, R. B. Walker, and E. F. Hayes, J. Chem. Phys. **110**, 6673 (1999).
[10] O. I. Tolstikhin, S. Watanabe, and M. Matsuzawa, J. Phys. B **29**, L389 (1996).
[11] H. Han, Y. Li, X. Zhang, and T. Shi, J. Chem. Phys. **128**, 244314 (2008).
[12] H. Suno, J. Chem. Phys. **134**, 064318 (2011).
[13] H. Han, Y. Li, and T. Shi, J. Chem. Phys. **134**, 194307 (2011).
[14] M. M. Liu, H. L. Han, C. B. Li, and S. H. Gu, Phys. Rev. A **88**, 042503 (2013).
[15] J. Macek, J. Phys. B **1**, 831 (1968).
[16] R. A. Aziz and M. J. Slaman, J. Chem. Phys. **94**, 8047 (1991).
[17] K. T. Tang and J. P. Toennies, J. Chem. Phys. **118**, 4976 (2003).
[18] Y. Li, Q. Gou, and T. Shi, Phys. Rev. A **74**, 032502 (2006).
[19] C. de Boor, *A Practical Guide to Splines* (Springer, New York, 1978).
[20] C. A. Parish and C. E. Dykstra, J. Chem. Phys. **101**, 7618 (1994).
[21] I. Røeggen and J. Almlöf, J. Chem. Phys. **102**, 7095 (1995).
[22] Y. Li, W. Zhang, Q. Gou, H. Song, and T. Shi, Phys. Rev. A **82**, 022515 (2010).
[23] Y. Li, D. Huang, Q. Gou, H. Han, and T. Shi, Phys. Rev. A **84**, 014501 (2011).
[24] Y. Li, H. Song, Q. Gou, H. Han, and T. Shi, Phys. Rev. A **79**, 024501 (2009).
[25] Y. D. Liu and P.-N. Roy, J. Chem. Phys. **121**, 6282 (2004).
[26] D. López-Durán, R. Rodríguez-Cantano, T. González-Lezana, G. Delgado-Barrio, P. Villarreal, and F. A. Gianturco, Phys. Rev. A **86**, 022501 (2012).
[27] M. Keil, L. J. Danielson, and P. J. Dunlop, J. Chem. Phys. **94**, 296 (1991).
[28] H. Bachau, E. Cormier, and P. Decleva, Prog. Phys. **64**, 1815 (2001).